Effect of Dual Pore Size Architecture on In Vitro Osteogenic Differentiation in Additively Manufactured Hierarchical Scaffolds

Author

Ratheesh, Greeshma, Shi, Mengchao, Lau, Patrick, Xiao, Yin, Vaquette, Cedryck

Published

2021

Journal Title

ACS Biomaterials Science & Engineering

Version

Accepted Manuscript (AM)

DOI

10.1021/acsbiomaterials.0c01719

The Effect of Dual Pore Size Architecture on *In Vitro* Osteogenic Differentiation in Additively Manufactured Hierarchical Scaffolds

Greeshma Ratheesh[1], Mengchao Shi[1], Patrick Lau[1], Yin Xiao[1,2], Cedryck Vaquette[3]

[1]Institute of Health and Biomedical Innovation, Queensland University of Technology, 60 Musk Avenue, Kelvin Grove, Queensland 4059, Australia

[2]Australia-China Centre for Tissue Engineering and Regenerative Medicine (ACCTERM), Queensland University of Technology

[3]School of Dentistry, The University of Queensland (UQ)

Abstract:

The combination of macro and micro-porosity is a potent manner of enhancing osteogenic potential, but the biological events leading to this increase in osteogenesis are not well understood. In this study, we investigated the effect of a dual pore size scaffold on physical and biological properties with the hypothesis that cell condensation is the determining factor for enhanced osteogenic differentiation. To this end, a hierarchical scaffold possessing a dual (large and small) pore size was fabricated by combining two additive manufacturing techniques; melt electrospinning writing (MEW) and fused deposition modelling (FDM). The scaffolds showed a mechanical stiffness of 23.22±1.46 MPa similar to the FDM control scaffold while the hybrid revealed an increased specific surface area of 1.43±0.06m^2/g. The scaffold was cultured with primary osteoblast cells for 28 days which showed enhanced cell adhesion and proliferation. The hierarchical structure was also beneficial for in vitro alkaline phosphate activity, mineralisation and showed an increased expression of osteogenic protein and genes. Mesenchymal condensation markers related to osteoblastic differentiation (CDH2, RhoA, Rac1, Cdc42) were upregulated in the hybrid construct demonstrating that the MEW membrane provided an environment more suitable for the recapitulation of cell condensation which in turn lead to higher osteogenic differentiation. In summary, this study demonstrated that the hierarchical scaffold developed in this paper leads to a significant improvement in the scaffold properties such as increased specific surface area, initial cell adhesion, cell proliferation and in vitro osteogenesis.

Keywords: melt electrospinning writing (MEW), fused deposition modelling (FDM), hierarchical scaffold, osteogenesis, dual-scale scaffold

1. Introduction

Additive manufacturing has become a prominent technology for scaffold fabrication in biomedical engineering. 3D printing and more particularly Fused Deposition Modelling (FDM) is one of the most widely used methods for the creation of scaffolds targeted to bone regeneration.[1-3] FDM exerts excellent control over scaffold design, internal architecture arrangement, porosity and pore sizes which are usually in the macroscopic range. The macroscopic interconnected porosity is desirable for a bone regeneration application as it allows efficient diffusion of nutrients and oxygen in vitro while facilitating formation of the vasculature, essential for osteogenesis to occur in vivo. Therefore, the optimal pore size of scaffold for bone regeneration ranges from 400 to 600 microns as several studies previously reported for a variety of scaffold types and biomaterials.[4-6] In the context of a tissue engineering strategy, whereby cells are cultured in vitro in a 3D construct prior to implantation, a compromise in the pore size is needed for simultaneously enabling in vitro maturation/differentiation and in vivo revascularisation. Indeed, 3D-printed scaffolds with highly ordered internal arrangements and macroscopic pores, required for proper in vivo vascularisation, are notoriously difficult to efficiently and homogenously seed with cells.[7] Several technological solutions have been implemented for enhancing initial cell adhesion,[8-12] however cell seeding efficacy remains poor for 3D-printed scaffolds.[13] In addition, the pore size of 3D constructs has a direct influence on cell proliferation and differentiation as previously demonstrated.[14-16] While there exits some contradictory results in the literature, it seems that a small pore size of around 100-300 microns is the most appropriate dimension for enhancing in vitro osteogenic differentiation.[14-15, 17]

As seen here, the pore sizes required for in vitro osteoblastic differentiation and in vivo osteogenesis are significantly different and lead to inadequate tissue engineering construct maturation characterised by reduced in vitro osteogenic differentiation in the context of a cellularised scaffold with a large pore size.

Therefore, the fabrication of a hybrid scaffold featuring small pore sizes, in the range of those suitable for in vitro osteogenic cell differentiation, and large pore sizes, desirable for in vivo vascularisation, is sound and can potentially increase the overall regenerative capacity of the resulting tissue engineered construct. The manufacturing of hierarchical scaffolds is generally achieved by combining 3D-printing and various iterations of electrospinning for obtaining constructs whereby a thin small pore size electrospun membrane is intercalated between two 3D-printed layers.[18-33] These technologies were developed and implemented firstly for enhancing cell seeding efficiency as the small pore size electrospun membrane acts as a net ensuring higher cell attachment when the seeding solution flows through the macropores of the constructs. While increased cell adhesion and proliferation have been reported in the majority of these studies,[21, 34] little is understood on the osteogenic capacities of such hybrid constructs possessing dual pore sizes.

In this study, we adopted a unique scaffold fabrication technique by combining two different additive manufacturing processes namely melt electrospinning writing (MEW) and fused deposition modelling (FDM) creating a hierarchically structured scaffold. The study focuses on understanding the effect of the scaffold hierarchical architecture on osteoblast proliferation, differentiation, their ability to generate mineralized matrix. The study also proposes a potential explaining and mechanism responsible for the increased osteogenic differentiation.

2. Materials and methods

2.1 Scaffold fabrication by additive manufacturing technologies

The scaffolds were fabricated in a two-step process combining two different additive manufacturing techniques, melt electrospinning writing (MEW) and fused deposition modelling (FDM). The first step involved the preparation of melt electrospun writing membranes using medical grade polycaprolactone (PCL) (Purasorb- PC12, Corbion). PCL pellets were melted in the electrospinning cartridge placed at 75°C and extruded through a 21G blunt needle placed at 80°C at a pressure of 1.2 bar and subjected to an electrostatic field of 7.5 kV. Electrospun scaffolds with 10 layers were fabricated with a 0-90° layer by layer arrangement with a 100 µm fibre interspacing on a programmable stage translating at a velocity of 1200 mm/min using a spinneret-to-collector distance of 7 mm. The pore size of the membrane was selected based on both the literature [14-15, 17] and our previous research demonstrating that a small pore size between 100 to 300 microns enabled rapid cell colonisation of the melt electrospun membrane. [35-36] Therefore, a 100 microns pore size was utilised in order to rapidly attain a state of cellular condensation. The second step of the manufacturing process involved the utilization of Fused Deposition Modelling whereby the PCL was melted at a temperature of 100ºC and extruded in a dual pneumatic pressurised bioextruder. The molten polymer was extruded using a 21G nozzle with a lay down pattern of 0-90º at a speed of 300mm/min. The scaffolds were fabricated with a filament distance of 0.5mm and a layer height of 0.35mm to achieve 45(L) x 45(W) x 2.5(H) mm^3. The FDM process was performed in a sequential manner whereby melt electrospun written membranes were intercalated in between each of the FDM layer. Once an FDM layer was printed, the fabrication process was stopped, and a melt electrospun membrane was placed over the FDM scaffold prior to resuming the printing. For comparison purposes, a FDM control scaffold (without intercalated melt electrospun membranes) was manufactured using the conditions described above. ***Figure 1*** shows the schematic representation of scaffold fabrication process; hence two groups MEW+FDM and FDM were created; the hierarchical scaffold composed of melt electrospun membranes intercalated in the FDM scaffold and the control FDM scaffold. This two-staged method of fabrication was utilised over a direct electrospinning approach on the FDM due to the collector electrical isolation leading to charge build-up, preventing the deposition of melt electrospun fibres with a precise and specific pattern.

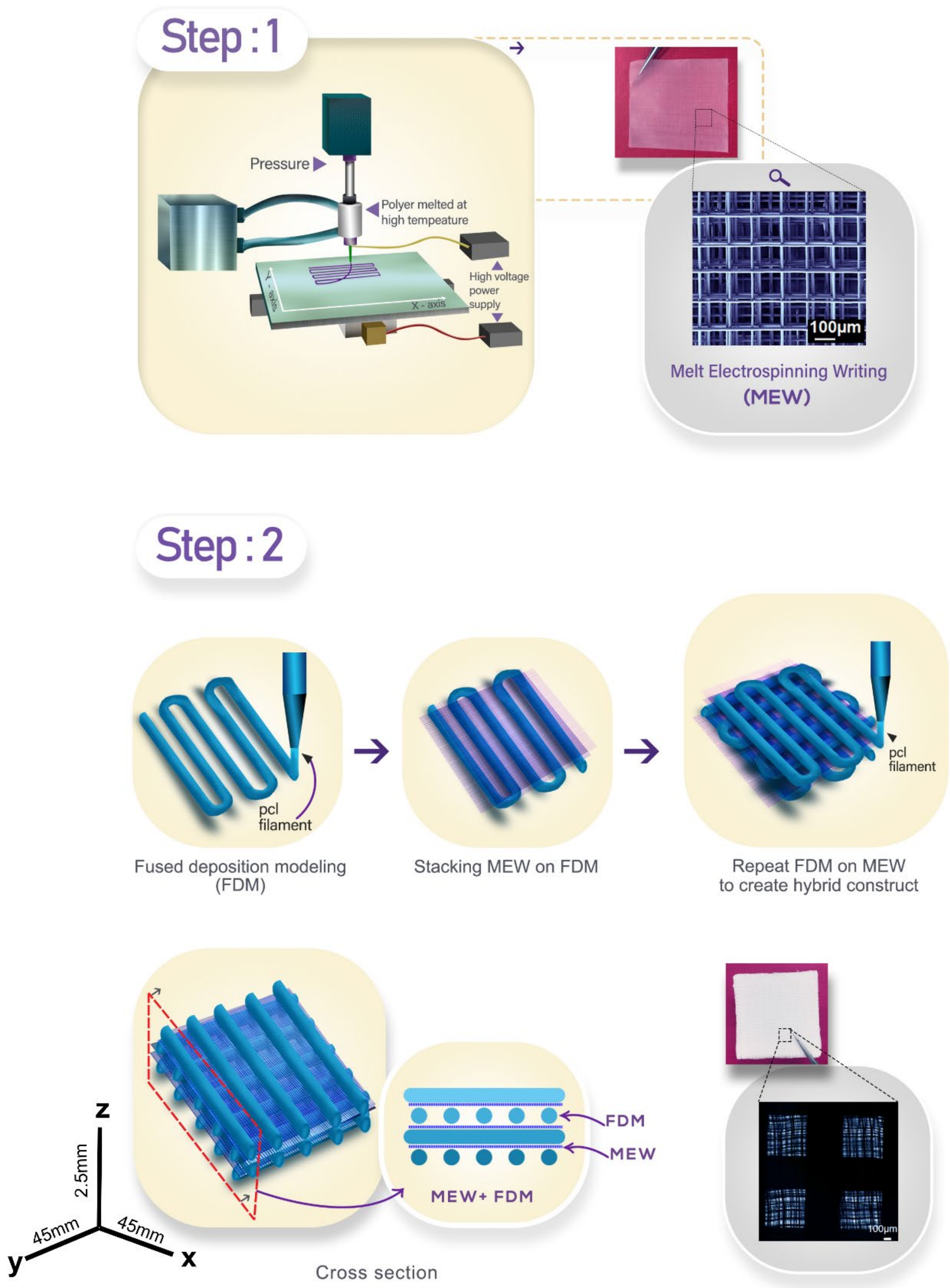

Figure 1: Schematic illustration of steps involved in the scaffold fabrication

2.2 Scaffold characterization

(i) Scaffold morphology

The scaffold morphology was examined for both the FDM and the MEW + FDM group using scanning electron microscopy (SEM) at 5 kV after gold sputter-coating. In order, to visualize and image the scaffold cross-sectional area, the constructs were submerged in liquid nitrogen and sectioned using a scalpel blade. Average fibre diameter and the average interfilament distance were determined using Image-J software from 5 SEM images tallying 50 measurements.

(ii) Microcomputed tomography

The scaffold porosity was analysed using a Micro-CT (µCT 40, SCANCO Medical AG, Bruttisellen, Switzerland) at resolution of 12µm, a voltage of 45kV, current of 177µA, and an integration time of 300ms with greyscale threshold of 30. The samples (n=3 per group) were coated with silver nitrate as a contrast enhancer prior to micro-CT.[37] Briefly, the samples of 6mm diameter (n=3 for each group) were soaked in silver nitrate (1%w/v in 100% ethanol) for 30 minutes, and subsequently immersed in a 10mM L-ascorbic acid solution (Sigma –Aldrich) and incubated for another 30 minutes. The samples were rinsed with water and the process was repeated once again and incubated overnight. Finally, the scaffold was washed in 80% ethanol and dried for micro-CT scanning.

The outlines of the scaffolds were manually segmented in order to determine the total volume of the scaffold and to calculate the porosity. Three-dimensional images were reconstructed from the scan using the micro-CT system software.

(iii) Compression testing

Mechanical compression tests were conducted using an Instron 5848 microtester fitted with a 500N load cell using experimental conditions similar or nearly similar to previous reports [1, 38]. The scaffolds (n=5 for each group) with the dimensions of 6mm diameter and a thickness of 2.5mm were compressed at a displacement rate of 0.6mm min^{-1}. The compressive Young's modulus of the scaffolds was determined from the initial linear portion of the stress versus strain curve.

(iv) Surface area by BET

The surface area of the scaffolds was measured by BET (Brunauer−Emmett−Teller Surface Area Analysis) at a relative pressure ranging from 0.05 to 0.3 (p/p^o) using an ASAP 2020 surface area and porosity analyser (Micromeritics Inc). The scaffolds (n= 25 for each group) were loaded into clean analysis tubes, which were weighed before and after loading. The analysis was performed at 77 K using Argon as adsorptive gas. Sample degassing was performed using freeze-drying process as the normal degas procedure using high temperature may cause melting of the PCL. After each freeze-dry run, the instrument was set to collect a 5-point isotherm for BET surface area analysis. The freeze-drying process was repeated till consistent BET results were observed.

2.3 In vitro characterization

(i) Cell source and extraction

Human joint tissue explant was obtained from patients undergoing knee or hip replacement surgery (ethical approval for the use of joint tissue was granted by The Prince Charles Hospital Human Research Ethics Committee, HREC, Queensland, Australia 1400001024). Written patient consent was obtained prior to tissue collection. The bone tissues were collected under sterile condition, minced and washed with phosphate buffer saline (PBS); and cultured in DMEM medium supplemented with 10% fetal bovine serum and 1% penicillin/streptomycin (basal medium). The extracted osteoblasts at passage 2 were used for all cell culture experiment.

(ii) Scaffold seeding and culture

Prior to seeding, the scaffolds of 6mm diameter were surface treated with 0.5M NaOH at 37ºC for 60 minutes, followed by 5 rinses in ddH_2O to increase surface hydrophilicity and promote initial cell attachment.[1, 39] The scaffolds were sterilized by a 30 min immersion in 80% ethanol followed by a 20 min UV sterilization on both sides of the scaffold. Then the scaffolds were seeded with 60µl of cell suspension (50,000 cells/scaffold) and incubated at 37ºC for 90 minutes, after which 1ml of basal medium was added to each scaffold. The scaffolds were cultured either in basal medium for up to 28 days for assessing viability, and proliferation or in osteogenic medium (basal medium supplemented with 2 mM β-glycerol phosphate (Sigma-Aldrich; Australia), 100µM L-ascorbic acid 2-phosphate(Sigma-Aldrich; Australia), and 10nM dexamethasone (Sigma-Aldrich; Australia)) for assessing gene expression and mineralization. Medium change was performed every 3 days.

(iii) Cell metabolic activity and DNA quantification

Cell metabolic activity was assessed using the non-destructive AlamarBlue™ (resazurin-based solution) cell viability assay (Invitrogen, Australia) assay at 1, 7, 14, 21, 28 days (n=5 at each timepoint). The scaffolds were placed in a new plate and 500 µL of a 10% vol/vol Alamar blue solution in DMEM medium were added to the wells and a 4 hour incubation at 37ºC in the incubator was performed. Thereafter, the Alamar blue solution was removed, the scaffolds were rinsed twice with PBS and 2mL of basal medium were added in order to continue the cell culture. The AlamarBlue solution's relative fluorescence (RFU value) (triplicates of 100 µL solution) was measured using a plate reader (BMG Labtech, CLARIOstar, Australia) at excitation wavelengths of 540/570nm and emission wavelengths of 580/610nm. A fully reduced AlamarBlue solution was used as a positive control, for which the AlamarBlue solution was autoclaved at 121ºC for 15 minutes as recommended by the manufacturer. Non-reduced AlamarBlue solution was used as negative control. The percentage reduction of AlamarBlue was calculated using the following equation

$$\%Reduction\ of\ AlamarBlue\ reagent = \frac{(Exprimental\ RFU\ value - Negative\ control\ RFU\ value)}{(100\%\ reduced\ postive\ control\ RFU\ value - Negative\ control\ RFU\ value)} \times 100$$

Cell proliferation was assessed by measuring DNA content was quantified by Pico green assay (Quant-iT™ PicoGreen™ dsDNA Assay kit, Invitrogen, Australia). At each time point the scaffolds (n=5 for each group) were washed with PBS and frozen at -80ºC for 48 hours. The constructs were digested using 500µL of Proteinase K (Invitrogen, Australia) at 60ºC for 12 hours. The solution was centrifuged at 2000 rpm for 5 minutes and the supernatant was diluted at a ratio of 1/20 in PBE. A triplicate of 100µL aliquot was transferred into a 96 well plate, to which 100µL of PicoGreen at a 1/200 dilution ratio was added. The plate was incubated for 5 minutes at room temperature in the dark, after which the fluorescence (excitation 485nm, emission 520nm) was measured using a fluorescence plate reader. A standard curve was plotted using λDNA (concentration of 10ng/mL to1µg/mL) to calculate the sample DNA content.

(iv) Cell viability and cell morphology

Cell viability was measured using a live/dead assay after 1, 7, 14, 21 and 28 days of culture in basal medium (n=3 per group and per timepoint). To this end, the scaffolds were washed twice in PBS and incubated for 5 minutes at 37ºC in FDA-PI solution (FDA: 10µg/ml; PI 5µg/ml in PBS). Thereafter, the scaffolds were washed with PBS and imaged using a Leica TCS SP5 Confocal Microscope at a maximum excitation/emission wavelength of 490-526 nm for FDA and 533-617nm for PI. The results were quantified using Fiji/Image-J software from three images at each time point for both groups. The percentage of living cells was calculated from the ratio of live cells (green cells) to the total number of cells (green and red cells).

The cellularized scaffolds were retrieved and processed for the assessment of cell attachment and morphology confocal laser microscopy and scanning electron microscopy (SEM) after 1, 7, 14, 21, 28 days of culture in basal medium. For confocal laser microscopy, the scaffolds (n=2 at each time point and for each group) were fixed in 4% (w/v) paraformaldehyde (PFA) for 30 min and transferred in PBS. Later, the cell membrane was permeabilised with 0.1% triton X solution for 20 minutes. Cell morphology was assessed by staining actin fibre and nuclei using a 0.8 U/ml rhodamine conjugated phalloidin (Invitrogen, Australia) and 5 µg/ml 4,6-diamino-2-phenylindole (DAPI, Invitrogen, Australia) in PBS for 20 minutes in dark at room temperature. The scaffolds were then washed with PBS to remove any excess stain. The samples were imaged using confocal laser microscopy as previously described at a maximum excitation/emission wavelength of 358/461nm for DAPI and 540/565nm for phalloidin.

SEM was performed after 28 days of culture and the constructs (n=2 for each group) were retrieved and fixed with 3% (w/v) glutaraldehyde followed by a thorough wash with PBS. The samples were subjected to sequential dehydration with graded ethanol series, immersed in hexamethyldisilazane (HMDS) for 60 min and subsequently dried prior to gold sputter-coating. The samples were imaged using the condition described above.

2.4 Gene expression of cells cultured on FDM and MEW+FDM scaffolds

Osteoblasts were isolated from bone tissue and seeded on the 3D printed scaffolds as previously described. To investigate osteoblastic differentiation, the cells were cultured in osteogenic media (basal medium supplemented with 2mM β-glycerolphosphate (Sigma-Aldrich; Australia), 100µM L-ascorbic acid 2-phosphate (Sigma-Aldrich; Australia) and 10nM dexamethasone (Sigma-Aldrich; Australia)) for 3, 7 and 21 days (n= 3 for each time point).

The total RNA was extracted by using TRIzol reagent (Invitrogen, Australia) according to the manufacturer's guidelines; and cDNA was synthesized using SensiFAST ^{TM} cDNA Synthesis Kit (Bioline, Australia). The synthesized cDNA was then added to the PCR master mix containing SYBR Green and specific primers (osteogenic markers ALP, RUNX2, COL 1, OCN, and OPN; cell condensation markers CDH2, Cdc42, Rac 1, and Rho A) as listed in Table 1. The mixture was then aliquoted into PCR array template. The RT-PCR was carried out in a thermal cycler (QuantStudio 7 Flex, Real-Time PCR System, ThermoFisher Scientific, Australia). The relative gene expression was calculated by normalizing the ΔC_T values to reference housekeeping gene GAPDH.

Table 1: Primers' sequence used in this study

Gene	Gene Symbol	Primers' Sequence
Alkaline Phosphate	ALP	TCTTCACATTTGGTGGATAC ATGGAGACATTCTCTCGTTC
Runt-related transcription factor 2	RUNX2	CATGGCGGGTAACGATGAA AGACGGTTATGGTCAAGGTGAAA
Collagen type 1	COL-I	GCAACATGCCAATCTTTACAAGAG CCATCATACTGAGCAGCAAAGTTC
Osteocalcin	OCN	GCAAAGGTGCAGCCTTTGTG GGCTCCCAGCCATTGATACAG
Osteopontin	OPN	TCACCTGTGCCATACCAGTTAA TGAGATGGGTCAGGGTTTAGC
N-Cadherin	CDH2	TAAAGAACGCCAGGCCAAAC

		TGGCATCAGGCTCCACAGT
Cell division control protein 42	Cdc42	GATGGTGCTGTTGGTAAA TAACTCAGCGGTCGTAAT
Ras-related C3 botulinum toxin substrate 1	Rac1	AAACCGGTGAATCTGGGCTT AGAACACATCTGTTTGCGGA
Ras homolog gene family, member A	Rho A	CCCAGATACCGATGTTATACTGATGT GGCACGTTGGGACAGAAATG

2.5 Osteogenic differentiation of cells: alkaline phosphatase activity and immuno-fluorescence staining

Alkaline phosphatase (ALP) activity was measured for the scaffolds (both FDM and MEW+ FDM) cultured in osteogenic medium at 7, 14, 21 and 28 days using a colorimetric assay. At each time point, the scaffolds (n=3 for each group) were retrieved and washed with PBS and the cell lysate was prepared with 200µl of 0.1%v/v Triton X-100 in 10mM Tris buffer (pH 7.5) for 10 minutes. The obtained lysate was mixed with 200µl assay buffer and centrifuged at 4°C at 10,000 rpm for 15 minutes. The supernatant was transferred to a new tube and a triplicate of 80µl sample solution was used. ALP activity was measured using the SigmaFAST™ kit as per the manufacturer's instruction using 50µL of a 5Mm *p* -nitrophenly phosphate solution (*p*NPP)) as phosphatase substrate. The plate was protected from light and incubated at 25ºC for 60 minutes. The *p*NPP reaction was stopped with 20µl of stop solution, and the absorbance was read at 405 nm using a plate reader (Benchmark™ Plus, Microplate Reader, Bio-Rad). The ALP absorbance was normalised with total protein content of each sample which was measured using BCA Protein assay kit (ThermoFisher Scientific, Australia).

Osteogenic differentiation of the cells was assessed by immunofluorescence staining after 3, and 7 days of culture in osteogenic medium. To this end, the scaffolds (n=3 for each group) were fixed with 4% paraformaldehyde for 10 minutes, permeabilized with 0.1% Triton X- 100 (Sigma-Aldrich, Australia) for 10 minutes. The samples were washed with PBS and blocked with 4% BSA (bovine serum albumin) for 1 hour at room temperature. The scaffolds were then incubated with rabbit polyclonal antibody against anti-ALP antibody (Cat.no. ab108337, Abcam, Australia) at 1:200 dilution in 1% BSA (Bovine serum albumin, Sigma, Australia) overnight at 4ºC. After incubation, the scaffolds were washed with PBS twice and incubated with secondary antibody (Donkey anti-rabbit 488, Abcam, Australia) at 1:500 dilution in 1% BSA (Bovine serum albumin, Sigma, Australia) for 1 hour at room temperature in dark. Lastly, the cell nucleus was stained with DAPI, the samples were washed twice with PBS and observed using confocal laser scanning microscopy (Leica TCS SP5 Confocal Microscope) at an excitation/emission wavelength of 495-519 nm for ALP and 358-461nm for DAPI and all imaging conditions were kept constant throughout the study. The fluorescence intensity was assessed quantitatively using Fiji/Image-J software as ratio of green pixels area to total cell number (number of blue objects) from three different images at each time point.

2.6 Mineralization of cells cultured on MEW+FDM and FDM scaffolds

Alizarin Red S staining was performed in order to assess the degree of mineralization in the FDM and MEW + FDM scaffold at 1,7,14, 21, 28 days of culture in osteogenic medium. At each time point, the scaffolds (n=3 for each group) were washed in PBS and fixed with 4% paraformaldehyde for 1 hour. The scaffolds were then washed with PBS, immersed in a 1wt% alizarin red S (Sigma-Aldrich, Australia) solution at pH 4.1 for 10 minutes. The unfixed dye was removed by gently rinsing the stained scaffolds with pure water until a clear solution was obtained (typically after 5 rinses). The samples were then air dried overnight and stored until use. Semi quantification of the alizarin staining was performed by solubilizing the dye using

300µL of a 50% acetic acid solution per scaffold. The scaffolds were placed on a shaker for 10 minutes to allow complete dissolution of dye and the solution was thereafter transferred to 1.5 mL Eppendorf tubes and vortexed for 30 seconds before the addition of 150 mL of 4 M NaOH to adjust the pH to 4.1. The tubes were centrifuged at 10,000 rpm for 10 min. Triplicates of 100 µL were placed in a 96-well plate and the absorbance was read at 405 nm. The mineralization was also examined by SEM after 28 days of culture in osteogenic medium. Briefly, the cells cultured on the scaffold were fixed with 3% (w/v) glutaraldehyde after 28 days, washed with PBS, dehydrated with ethanol series, air dried, sputter coated with gold and imaged using SEM as per the conditions previously described.

3. Statistical analysis

All the data were expressed as mean ± standard error of the experiments. The statistical significance was analysed using one-way ANOVA with LSD Post Hoc test. Otherwise, for data comparing only two means (such as mechanical properties, porosity and surface area study) an unpaired student t-test was utilized. The data was plotted using GraphPad Prism 7.00 – California or Microsoft Excel. In all the statistical evaluations p-values <0.05 was considered as statistically significant.

4. Results

4.1 Scaffold fabrication and physical characterization

An architecturally hybrid hierarchical 3D scaffold was fabricated by combining two additive manufacturing processes, Fused Deposition Modelling (FDM) and Melt Electrospinning Writing. SEM imaging of the FDM scaffold revealed a typical architecture for such scaffold consisting of large filaments with an average diameter of 530±34.37µm and an average interfilament distance of 450±67.77µm (***Figure 2 a, d, e***) creating an alternated 0-90º layer architecture. The MEW membrane showed a highly ordered structure composed of smooth fibre with an average fibre diameter of 7±0.84µm, and an average interfilament distance of 100±4.98µm (***Figure 2 b, d, e***). The combination of the FDM and MEW resulted in the fabrication of scaffolds with a dual pore size: with large pores created by the mechanically robust FDM filament into which smaller pores from the MEW membranes were intercalated in a layer by layer manner (***Figure 2 c***).

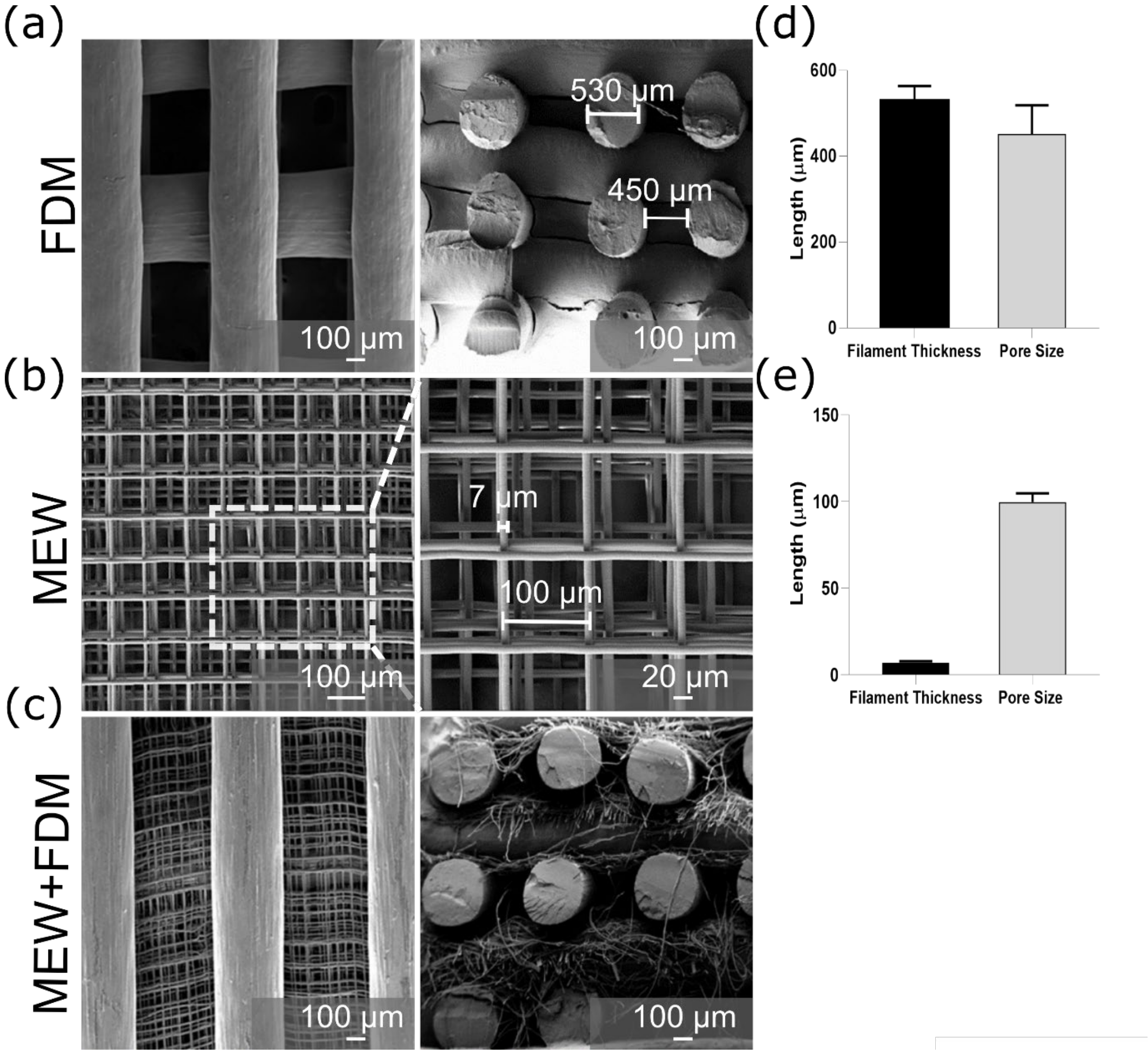

Figure 2: Morphology of the 3D printed PCL scaffolds using SEM (n=3): (a) Top and the cross-section view of 3D printed FDM scaffold (b) Representative image of MEW scaffold showing average fibre diameter and the interfilament distance, (c) Top and cross-section view of the 3D printed MEW+FDM scaffold with clear intact of the MEW in between the layers of

FDM, (d) Filament thickness and pore size of FDM scaffold, (e) Filament thickness and pore size of MEW scaffold.

The impact of the MEW membrane incorporation was investigated by compression testing and this demonstrated that both types of scaffold had similar compressive properties as shown in ***Figure 3a and b.*** Indeed, both the FDM and the MEW + FDM displayed a typical compression curve of porous polymeric materials characterized by a gradual increase in the stress before reaching an inflexion (around 20% strain) corresponding to densification phase as described by Gibson and Ashby [40] and corresponding the collapse of the FDM pore.

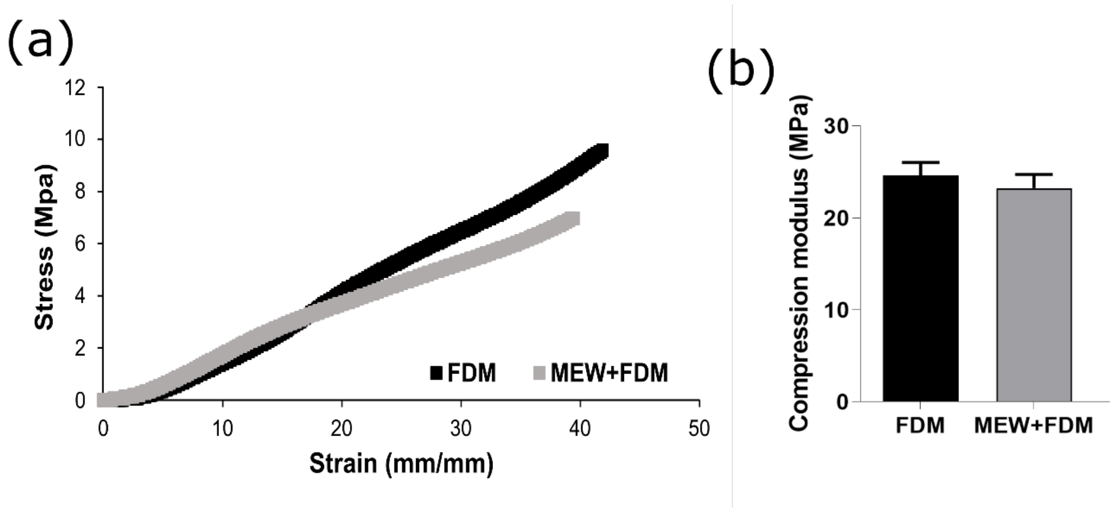

Figure 3: Compression testing: (a) stress-strain curve of the 3D printed scaffold, (b) Compressive young's modulus of the FDM and MEW+FDM scaffolds determined from the initial linear portion of the stress-strain curve showing no significant difference (n=5)

The compressive Young's modulus (calculated from the initial linear region of the stress stain curve) (***Figure 3a***) of both group was in the range of 25 MPa and no statistical difference was noted with the MEW+FDM (FDM: 24.6±1.4 MPa; MEW+FDM: 23.2±1.5 MPa) as shown in ***Figure 3b***. Similar observations were found in the porosity analysis, where the FDM (50.5 %±0.4) and MEW+FDM (47.8% ±2.2) did not show any significant difference (***Figure 4a-c***). However, the presence of the MEW membrane greatly affected the scaffold specific surface area as the BET analysis demonstrated. Indeed a 5-fold increase in this parameter was observed with the MEW+FDM surface area culminating at 1.43 ± 0.06 $m^2.g^{-1}$ while the FDM was at 0.03 ± 0.01 $m^2.g^{-1}$ scaffold (***Figure 4d***).

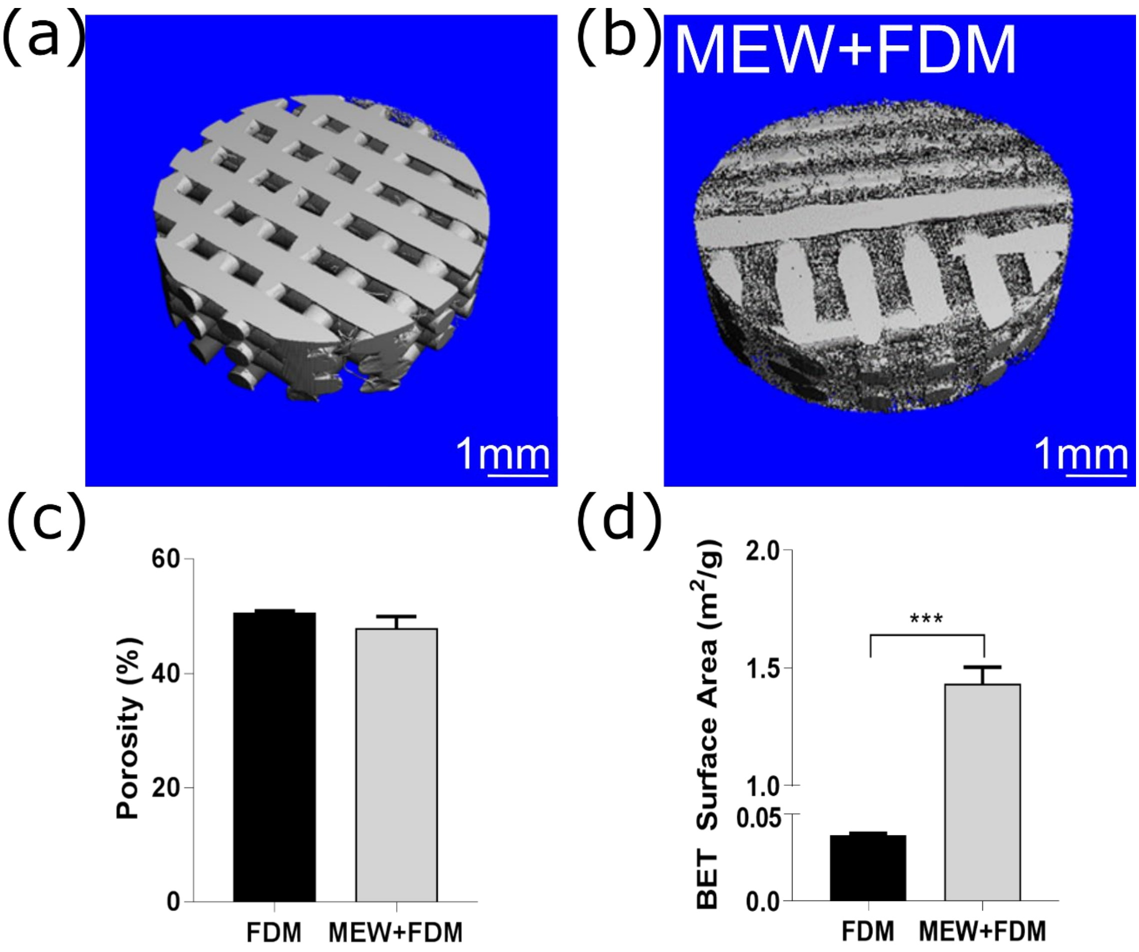

Figure 4: (a) Representative 3D image of Micro-CT on FDM scaffold, (b) Representative 3D image of Micro-CT on MEW+FDM scaffold, (c) Percentage porosity calculated from the Micro-CT analysis showing no significant difference, (d) BET surface area analysis on FDM and MEW+FDM scaffold. Data represented as mean ± SED (*: $p< 0.05$; **: $p<0.01$; ***: $p<0.001$)

4.2 In vitro characterization

(i) Cell metabolic activity and proliferation

Primary human osteoblasts were cultured on the 3D printed scaffold for 28 days and the cell metabolic activity was assessed by Alamar Blue assay and the DNA content was also measured. At 24 hours post-seeding, the percentage reduction of the Alamar Blue corresponding to cell metabolic activity was below 5% for both group where MEW+FDM displayed a significantly higher activity than the FDM group (***Figure 5a***). With longer culture time, the cell metabolic activity gradually increased, however this parameter was consistently and significantly higher in the MEW + FDM group when compared to the FDM group. A similar trend was observed for the DNA content, whereby higher DNA content in the MEW+FDM was observed although it did not reach statistical significance at the early time points of 1 and 7 days. While cell number increased in both groups, the DNA content in the MEW + FDM was remarkably and significantly higher from day 14 to day 28, with a 4-fold difference when compared to the FDM group (***Figure 5b***). We further calculated the DNA fold change between consecutive time points and between Day 1 and Day 28 (***supplementary Figure 1***). This still clearly demonstrated that the hybrid construct resulted in enhanced proliferation overall with a10 fold increase in the MEW+FDM compared to 7 fold increase in the FDM.

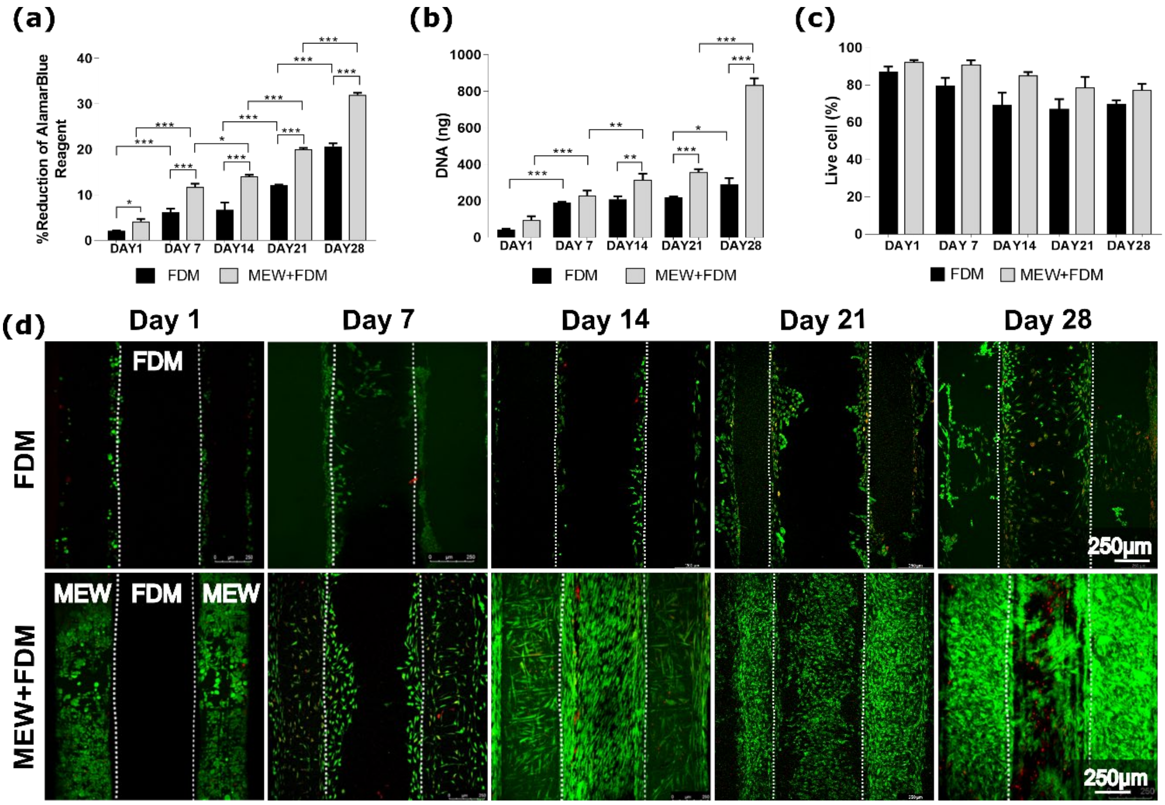

Figure 5: (a) Cell metabolic activity analysis by Alamar blue assay (n=5), (b) DNA quantification by Pico green assay (n=5), (c) Cell survival percentage assessed quantitatively as ratio of live cells to total cell, (d) Representative confocal laser microscopy image showing live/dead cells after 1, 7, 14, 21 and 28 days of culture and staining with FDA (green-live) and PI (red-dead) (n=3). Data represented as mean ± SED (*: $p< 0.05$); (**: $p<0.01$); (***: $p<0.001$)

Live dead assay demonstrated that the cells maintained an initial high level of cell viability around 90% which slightly decreased afterwards to 70-80% as shown in ***Figure 5c and d***. There were no significant differences in cell viability between the groups, even when the MEW FDM scaffold demonstrated extensive cell proliferation which results in filling the pores of the MEW membrane. This indicated that the diffusion of oxygen and nutrients were not impeded despite the presence of densely cellularized MEW membranes between each layer of the FDM scaffold.

Confocal fluorescence microscopy provided a visual confirmation of enhanced cell seeding capacity of the MEW+FDM scaffold as higher number of cells were observed in this group at 24-hour post-seeding. Interestingly, the cells were mostly located in the MEW membrane as shown in ***Figure 6a*** demonstrating that the electrospun written membranes acted as a net to capture the cells and were responsible for the increased seeding efficacy. In comparison, the FDM scaffold did only display a few cells that were attached the PCL struts. For longer culture time points, the cell colonized all portions of the scaffold and had wrapped the FDM filament in both groups, however the cells spread and elongated along the melt electrospun fibres (***Figure 6a***). Scanning Electron Microscopy of scaffold cultured with osteoblasts revealed that the cell spread around individual fibres on the hierarchical scaffold, whereas the FDM scaffold showed cell growth uniquely on the filaments (***Figure 6b and c***).

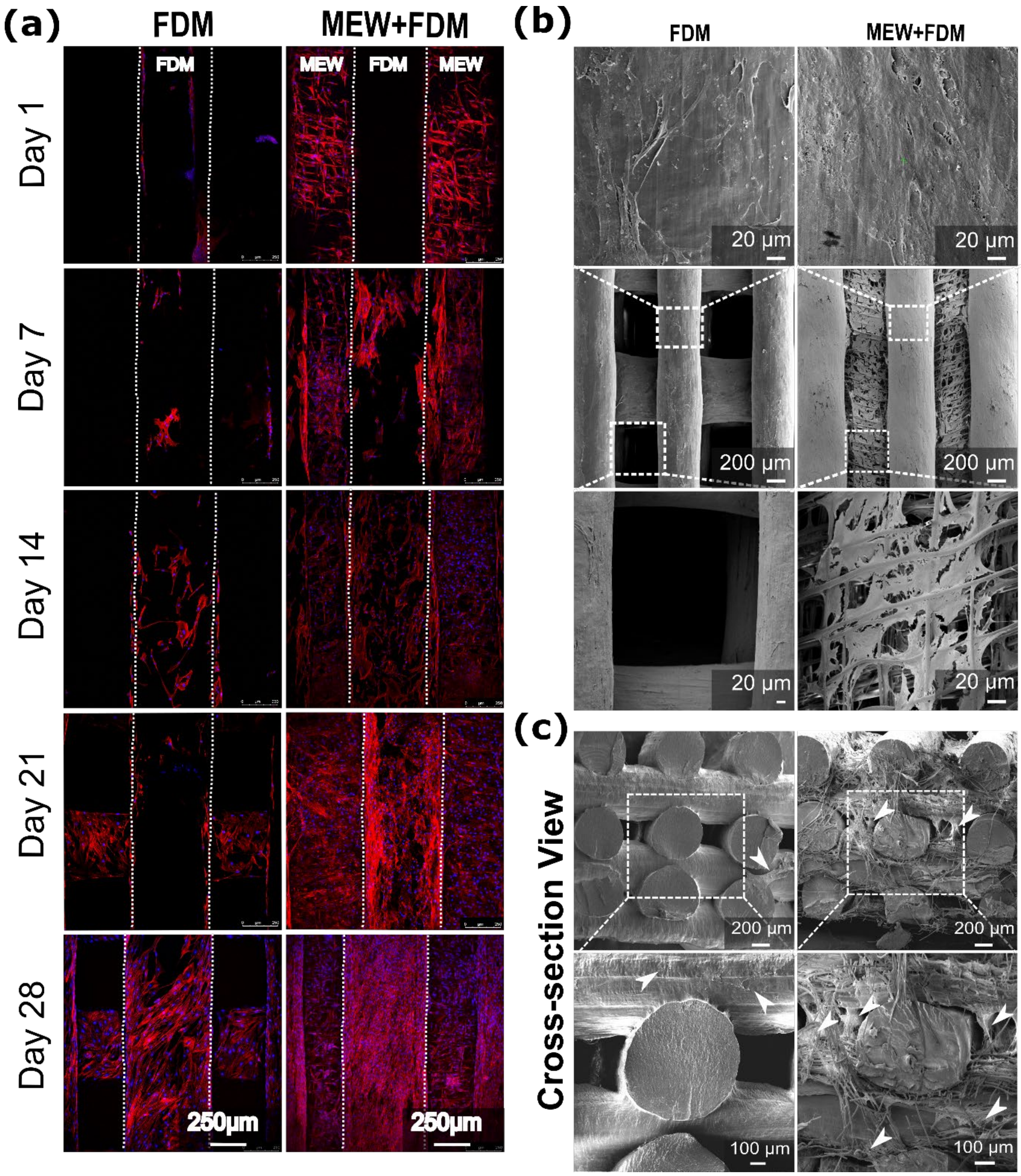

Figure 6: (a) Representative confocal laser microscopy image of human osteoblast cells cultured for 1, 7, 14, 21 and 28 days and stained for actin (Phalloidin) and nucleus (DAPI), (b) Representative SEM micrograph of osteoblast cells cultured for 28 days on 3D printed scaffold, (c) Representative cross-section view of 3D printed scaffold cultured with osteoblast cells for 28 days.

(ii) Gene expression

The scaffolds were seeded with human osteoblasts and cultured for 3, 7 and 21 days in osteogenic medium. The expressions of osteogenic related genes such as alkaline phosphate (ALP), runt-related transcription factor2 (Runx2), osteopontin (OPN), osteocalcin (OCN), and collagen type I (COL-I) were assessed by qRT-PCR. As shown in ***Figure 7a,*** the expression of ALP gradually increased from day 3 to day 21 for both the FDM and the MEW+FDM. At day 7, the MEW+FDM had higher ALP expression although it did not reach statistical significance. Runx2 demonstrated a similar expression profile with a gradual increase over time, indicating that the osteoblasts were not a homogenous cell population and had various levels of osteogenic commitment. Interestingly, RUNX2 expression was significantly higher in the FDM +MEW group at day 7 suggesting that osteogenic commitment in the FDM scaffold was delayed. COL-I demonstrated a significant increase in expression over the in vitro culture, and although the FDM had a significantly higher Col 1 expression at day 3, this profile was inverted at day 21 and the MEW + FDM displayed a 2-fold higher expression when compared to the FDM group. OCN demonstrated a similar pattern of gradual increase, starting with an even level of expression at early time points followed by significantly increased expression for the MEW+FDM group at day 21. OPN expression was significantly higher at day 3 in the MEW+FDM group followed by a sharp decrease in both groups at day 7 and a slight increase at day 21 when compared to the previous time point.

The expression of genes involved in mesenchyme condensation leading to osteogenesis was also investigated. This revealed that these genes CDH2, Cdc42, Rac1 and RhoA had significantly higher expression in the MEW + FDM group at day 7 (***Figure 7b***), indicating that earlier, enhanced cell maturation and possibly condensation occurred in the hybrid construct. This potentially explains the superior capacity if the MEW + FDM at inducing in vitro osteoblastic differentiation.

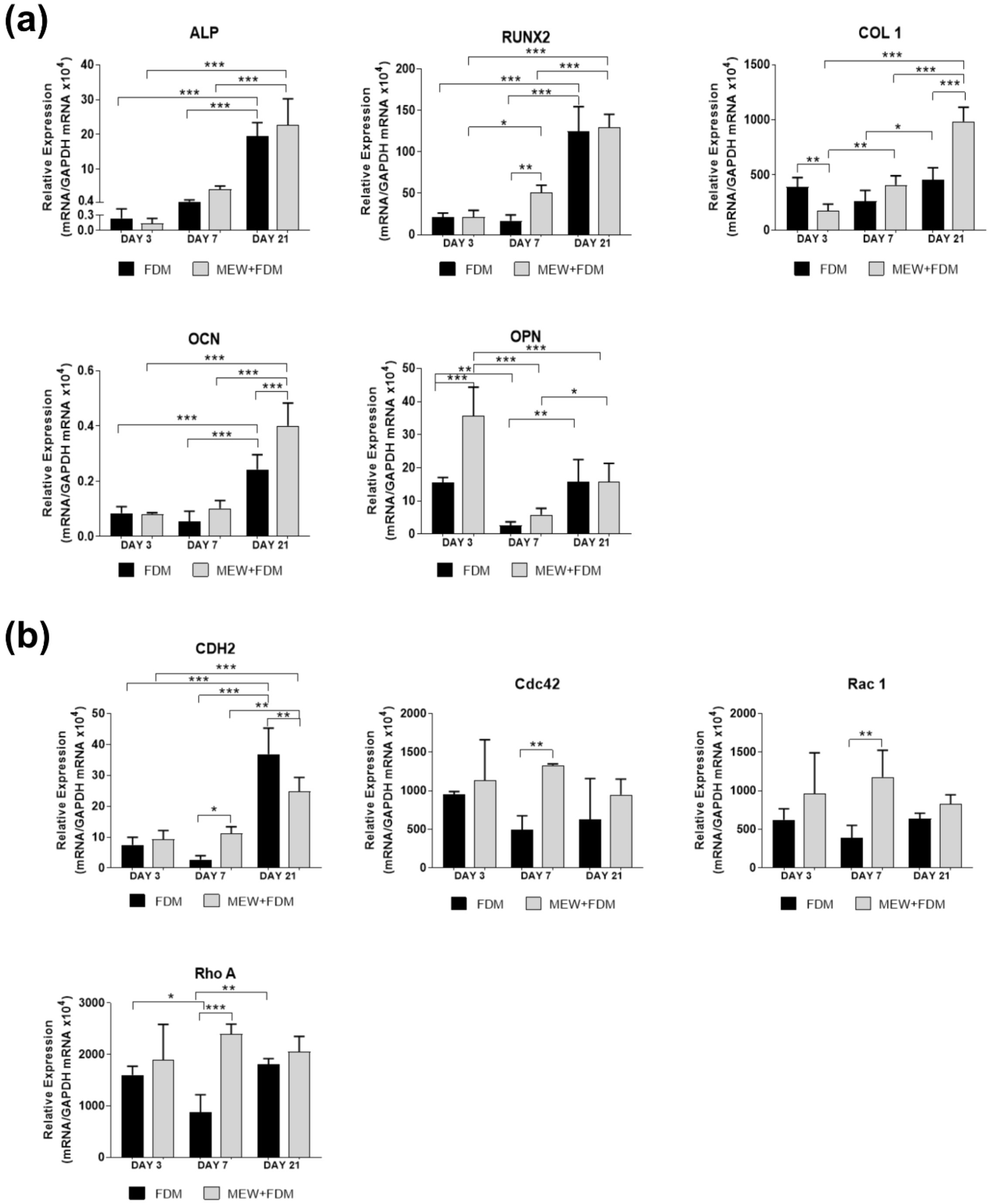

Figure 7: Gene expression using RT-PCR of human osteoblast cells cultured in osteogenic medium for 3,7 and 21 days on 3D printed scaffold (a) osteogenic markers (b) cell condensation markers (n=3). Data represented as mean ± SED. Data represented as mean ± SED (*: p< 0.05); (**: p<0.01); (***: p<0.001).

(iii) Osteogenic differentiation of cells: alkaline phosphatase activity and immuno-fluorescence staining

The commitment to osteogenic differentiation was also analysed at the protein level by measuring ALP activity normalized to the total protein content at various time points. The ALP activity in the MEW+FDM scaffold was consistently and significantly increased when compared to the FDM scaffold after 7, 21 and 28 days of culture (***Figure 8a*).** This indicated that the architecture of the FDM+MEW scaffolds, enabling high cell proliferation and condensation, was also beneficial for ALP production. This finding was confirmed by immunofluorescence staining towards ALP at the early time points of 3 and 7 days, whereby the ALP staining integrated pixel intensity normalised by cell number was significantly higher in the FDM+MEW as shown in ***Figure 8b and c***.

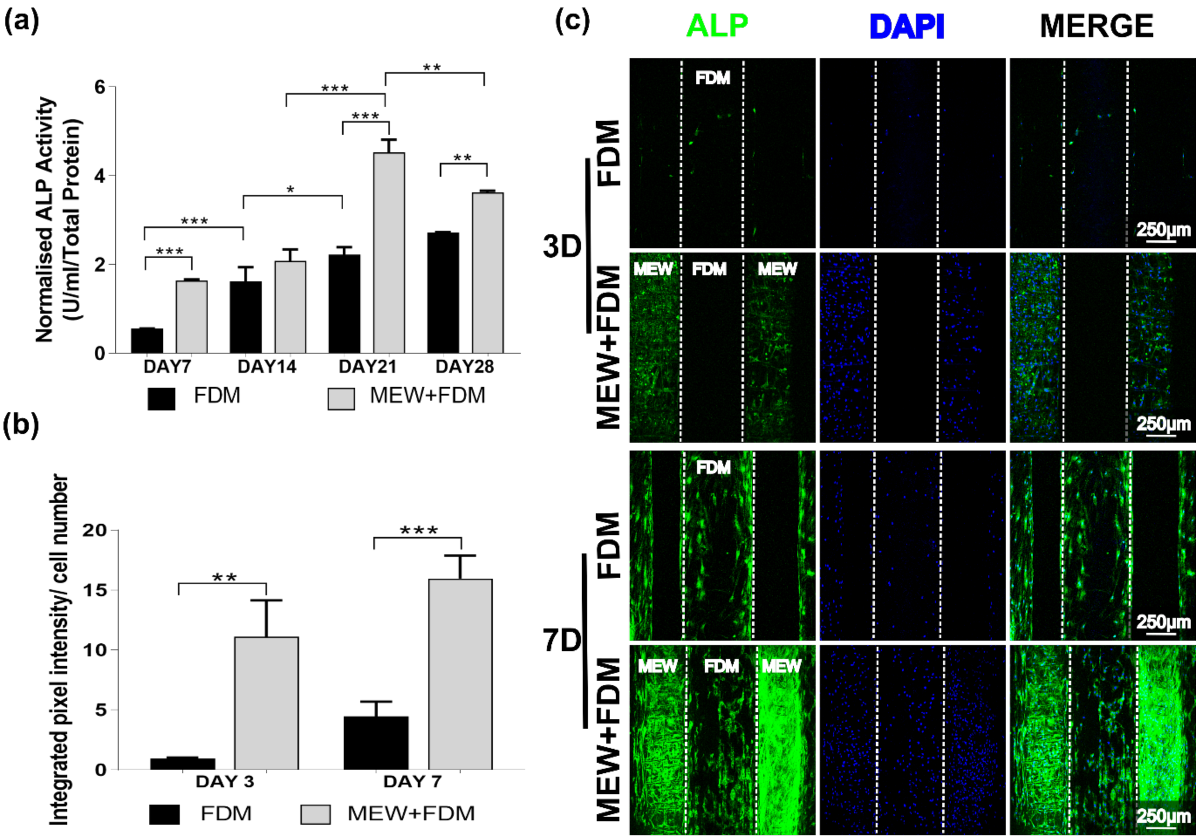

Figure 8: (a) Alkaline phosphatase activity of human osteoblast cells cultured on 3D printed scaffold for 7, 14, 21 and 28 days (n=5), Immunofluorescence staining for ALP on the 3D

printed scaffold after 3 and 7 days of culture in osteogenic medium: (b) Fluorescence intensity assessed quantitatively as ratio of green pixels to total cell number, (c) Representative confocal laser microscopy image of FDM and MEW+FDM scaffold stained for ALP after 3 and 7 days (n=3). Data represented as mean ± SED (*: $p< 0.05$); (**: $p<0.01$); (***: $p<0.001$)

(iv) Mineralization of cells cultured on MEW+FDM and FDM scaffolds

Cell mineralization was assessed by Alizarin red staining after 1, 7, 14, 21 and 28 days of culture. A gradual increase in mineralization was observed for both groups throughout the entire experiment. Interestingly, the FDM+MEW samples displayed mineralized nodules as early as 7 days post-seeding (**Figure 9a**) whereas mineralization only appeared after 14 days post-seeding in the FDM groups. In consequence, alizarin Red staining quantification demonstrated a significant increase from day 14 in the MEW+FDM specimens (***Figure 9b***). The level of mineralization was further visualized by scanning electron microscopy after 28 days of culture, revealing that the cells had formed mineralized matrix in both types of scaffold (***Figure 9c***).

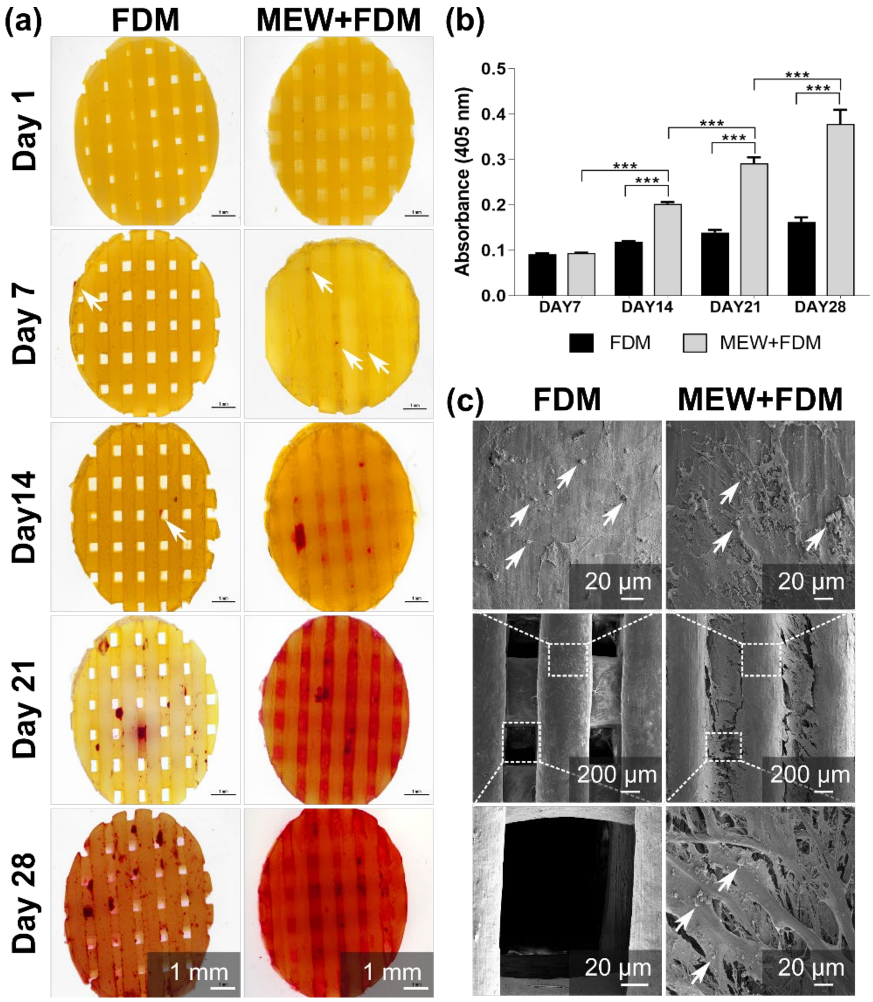

Figure 9: (a) Alizarin Red S staining of human osteoblast cells cultured in osteogenic medium for 1, 7, 14, 21 and 28 days on 3D printed FDM, MEW+FDM scaffold (n=3), (b) Quantification of Alizarin Red S staining by reading the absorbance at 405nm (n=3), (c) SEM micrograph of human osteoblast and mineralised particles after 28 days of culture in osteogenic medium (n=3) Data represented as mean ± SED (*: p< 0.05); (**: p<0.01); (***: p<0.001)

5. Discussion

This study reported on the manufacturing of an additively manufactured hybrid scaffold possessing a dual scale pore size. This was achieved by combining two additive manufacturing processes melt electrospinning writing (MEW) and fused deposition modelling (FDM) which resulted in the intercalation of highly ordered and porous melt electrospun membranes in between the fused deposited filaments consistently with previous reports.[16, 18, 20-30] This specific geometry, encompassing large pore sizes from the FDM structure and the smaller pores size of the MEW membranes, resulted in influencing the biological response of human osteoblasts. Previous studies have demonstrated that pore size, porosity and interconnected channels play a crucial role in osteogenic signal expression, differentiation, migration and bone formation.[41-43] While the macropores of the FDM enabled nutrient and oxygen supply to the core of the scaffold, the small pore size of the MEW membrane created a microenvironment suitable for excellent osteogenic differentiation. This was achieved while still maintaining access to oxygen and nutrient as shown by the consistent increase in metabolic activity and DNA content throughout the experiment consistently to previous reports. [36, 44-45] In addition, there was no difference in cell viability between the FDM and hybrid construct demonstrating that the presence of the small pore size membrane did not induce a significant impediment in the oxygen and nutrient diffusional processes.

This is also consistent with previous reports using hierarchical constructs whereby the presence of a smaller pore size component in a 3D-printed scaffold enhanced in vitro osteogenic differentiation,[23, 29] although contradictory findings can also be found in the literature.[26-27, 46] In the present study, the enhancement of osteogenic differentiation characterised at the protein level by increased ALP secretion and higher osteogenic markers gene expression (at day 7 for RUNX2 and at later timepoints for Col 1 and OCN), was concomitant and/or possibly induced by higher cell to cell contact in the MEW + FDM scaffold as shown by the increased N-Cadherin (or CDH2) gene expression at day 7. N-Cadherin is an essential marker of cell condensation and it has been shown to direct osteoblastic differentiation with a high initial expression followed by a decrease, conventionally associated to the formation of osteocyte.[47] Therefore, the increased and intimate cell to cell contact, principally mediated by high N-Cadherin expression, seems to recapitulate the necessary step of cell condensation for osteogenesis during skeletal development.[48-49] In addition, several other markers such as RhoA, Rac1 and Cdc42 involved in cell condensation prior to osteogenesis were also upregulated at day 7, further suggesting that the presence of the MEW membrane resulted in an early onset of condensation which subsequently increased the cells osteogenic commitment. These genes regulate the production of molecules that are part of the Rho family of small GTPases and regulate cell shape, adhesion, migration, proliferation[50-52] and are also known to directly influence the osteogenic process.[52-55] Although the present study has reported an upregulation of these genes (CH2, Cdc42, RhoA and Rac1) suggesting increased commitment towards cell condensation at the 7 day time point, their translation to protein production may still require further investigations.

Nevertheless, the utilisation of MEW membrane in the hybrid construct enhanced osteogenic differentiation and this was mediated by the higher state of cellular condensation induced by the small pore size of the MEW membranes. A striking evidence is also found in the comparison of two studies assessing ectopic bone formation subsequent to in vitro culture of ovine osteoblasts seeded in either a large pore size 3D-printed scaffold[1] or a smaller pore size (100-200 microns) melt electrospun construct.[36] Indeed, with similar cell type and length of in vitro differentiation, the small pore size scaffold resulted in extensive bone formation[36] while the large pore size was solely infiltrated by fibrous tissue.[1] This may have been caused by the macroscopic features of the 3D-printed scaffold imparting a lower surface area which did not allow enough cellular interaction, proliferation and condensation for reaching a threshold resulting in bone formation once implanted. Whereas high cell number and increased cell to cell contact, known to affect cell differentiation towards the osteoblastic lineage,[47] were present in the case of the smaller pore size scaffold and thus enabled in vivo osteogenesis similarly to the hybrid construct developed in the present study. In addition, the presence of the MEW membranes drastically increased the surface area available for cell attachment and this consequently resulted in higher cell seeding efficiency and proliferation consistently with previous reports.[22, 24, 30, 56-57] Ming *et al.* demonstrated that electrospun scaffold with a uniform structure and high specific surface area initiated faster cell attachment and served as a good substrate for rapid tissue regeneration.[58] These previous reports also demonstrated that the presence of a smaller pore size membrane in the hundreds of microns range still allows osteogenesis and vascularisation to occur in cell laden or growth factor loaded tissue engineered scaffolds[35-36, 59]. While the effect of the fibre diameter on in vitro osteogenic differentiation was outside the scope of this present study, the utilisation of sub-micrometric fibres in the electrospun membrane may be beneficial for further increasing the construct osteogenic potential as previously demonstrated. [60] In addition, these findings may be extrapolated to other aliphatic polyester, commonly utilised in tissue engineering for bone regeneration, since an architectural cue (that is, the small pore membrane) is mainly responsible for the increased cell condensation.

The manufacturing of the MEW + FDM scaffold was performed in two separate steps involving the electrospinning of the membrane which was then intercalated between the FDM layers during the printing process. This strategy was in contrast to previous reports whereby an electrospinning apparatus was added to the 3D-printed in order to alternatively and directly electrospin a thin membrane over the FDM layers previously deposited.[18, 20, 24-29] The implementation of such a strategy in the context of melt elelctrowriting, although not impossible, is technically challenging. Wei et al. were able to incorporate a melt electrospinning head to their 3D-printer but reported multiple issues related to the deposition of a hot microfilament over the large gap formed by the FDM struts resulting in important sagging of the fibres.[28] Furthermore, the addition of multiple layers was reported to significantly disturb the electrostatic field necessary for the formation of a stable melt electrospun jet, thus potentially impeding the ordered deposition of microfibers.[28] Our strategy circumvented these limitations and resulted in the fabrication of a hybrid construct whereby the melt electrospun fibre orientation was perfectly maintained. In the present study the fabrication of the scaffold required a precise control of the temperature of the FDM printing head in order to avoid melting of the melt electrospun fibres while still ensuring appropriate fusion of the FDM layer for firmly anchoring the MEW membrane within the construct. The fusing of the adjacent layers also resulted in the maintenance of the compressive mechanical properties which is in accordance with several reports using dual scale hybrid scaffolds.[20, 22] The combination of melt electrospinning writing and FDM enabled a totally solvent free manufacturing process hence avoiding the presence of residual solvent in the electrospun fibres[44, 61-62] which can create concern for regulatory approval. Indeed, solution based electrospinning was utilised in the majority of the previous studies reporting the fabrication of hierarchical hybrid constructs, and this created another limitation as the very small pore size of the resulting solution electrospun membrane impeded cell migration through the layers of the scaffold as previously reported.[61, 63] This limitation was circumvented by using near filed electrospinning[28] or by electrospinning for a short period of time[24] in order to create an electrospun membrane with low fibre density, thus with larger pore sizes,[64] which in turn allowed cell migration and fully cellular colonisation. More recently, solution electrospinning was performed while translating the collector stage at higher velocity in order to partially cover the FDM layer and hence creating large gaps allowing cell migration. Another strategy consisted in bioprinted a cell laden alginate bioink within the construct thereby obtaining a homogenous cell distribution,[30] thus circumventing the limitations revolving around cell migration . In the present study, the MEW membrane had a pore size of 100µm which enabled the migration of the cells towards the adjacent layers, which resulted in homogenous and full colonisation of the hybrid construct without the utilisation of other more complex technical solutions.

6. Conclusion

In this study a unique hierarchical scaffold combining two printing strategies, melt electrospinning and the fused deposition modelling was fabricated. The melt electrospun fibres were intercalated successfully in between the PCL fused deposited filaments. The dual pore size of the hierarchical scaffold increased osteogenic commitment of human osteoblasts and this was mediated via the upregulation of genes involved in cell condensation for bone formation such as CDH2, RhoA, Rac1 and Cdc42. This study provides a deeper insight on the potential biological mechanisms that can enhance osteogenesis and can guide the design of scaffolds utilised in tissue engineering towards bone regeneration by incorporating an additional smaller pore size feature.

7. Acknowledgements

The authors would like to acknowledge the kind support by the ARC industrial transforming centre in additive biomanufacturing, QUT-IHBI for the 3D printing facility; Central Analytical Research Facility (CARF), QUT for the imaging facility.

8. Funding sources

The author gratefully acknowledges Queensland University of Technology (QUT) for the PhD research scholarship. The project is also supported by the ARC Training Centre in Additive Biomanufacturing IC160100026.

9. References

1. Poh, P. S. P.; Hutmacher, D. W.; Holzapfel, B. M.; Solanki, A. K.; Stevens, M. M.; Woodruff, M. A., In vitro and in vivo bone formation potential of surface calcium phosphate-

coated polycaprolactone and polycaprolactone/bioactive glass composite scaffolds. *Acta Biomater* **2016,** *30*, 319-333. DOI: 10.1016/j.actbio.2015.11.012.

2. Hutmacher, D. W.; Sittinger, M.; Risbud, M. V., Scaffold-based tissue engineering: rationale for computer-aided design and solid free-form fabrication systems. *Trends Biotechnol* **2004,** *22* (7), 354-362. DOI: https://doi.org/10.1016/j.tibtech.2004.05.005.

3. Hollister, S. J., Porous scaffold design for tissue engineering. *Nature materials* **2005,** *4* (7), 518-24. DOI: 10.1038/nmat1421.

4. Sicchieri, L. G.; Crippa, G. E.; de Oliveira, P. T.; Beloti, M. M.; Rosa, A. L., Pore size regulates cell and tissue interactions with PLGA-CaP scaffolds used for bone engineering. *J Tissue Eng Regen Med* **2012,** *6* (2), 155-62. DOI: 10.1002/term.422.

5. Karageorgiou, V.; Kaplan, D., Porosity of 3D biomaterial scaffolds and osteogenesis. *Biomaterials* **2005,** *26* (27), 5474-91. DOI: 10.1016/j.biomaterials.2005.02.002.

6. Entezari, A.; Roohani, I.; Li, G.; Dunstan, C. R.; Rognon, P.; Li, Q.; Jiang, X.; Zreiqat, H., Architectural Design of 3D Printed Scaffolds Controls the Volume and Functionality of Newly Formed Bone. *Adv. Healthc. Mater.* **2019,** *8* (1), 1801353. DOI: 10.1002/adhm.201801353.

7. Thevenot, P.; Nair, A.; Dey, J.; Yang, J.; Tang, L., Method to analyze three-dimensional cell distribution and infiltration in degradable scaffolds. *Tissue engineering. Part C, Methods* **2008,** *14* (4), 319-31. DOI: 10.1089/ten.tec.2008.0221.

8. van den Dolder, J.; Spauwen, P. H.; Jansen, J. A., Evaluation of various seeding techniques for culturing osteogenic cells on titanium fiber mesh. *Tissue engineering* **2003,** *9* (2), 315-25. DOI: 10.1089/107632703764664783.

9. Godbey, W. T.; Hindy, S. B.; Sherman, M. E.; Atala, A., A novel use of centrifugal force for cell seeding into porous scaffolds. *Biomaterials* **2004,** *25* (14), 2799-805. DOI: 10.1016/j.biomaterials.2003.09.056.

10. Nasrollahzadeh, N.; Applegate, L. A.; Pioletti, D. P., Development of an Effective Cell Seeding Technique: Simulation, Implementation, and Analysis of Contributing Factors. *Tissue engineering. Part C, Methods* **2017,** *23* (8), 485-496. DOI: 10.1089/ten.TEC.2017.0108.

11. Beşkardeş, I. G.; Aydın, G.; Bektaş, Ş.; Cengiz, A.; Gümüşderelioğlu, M., A systematic study for optimal cell seeding and culture conditions in a perfusion mode bone-tissue bioreactor. *Biochem. Eng. J.* **2018,** *132*, 100-111. DOI: https://doi.org/10.1016/j.bej.2018.01.006.

12. Blaudez, F.; Ivanovski, S.; Ipe, D.; Vaquette, C., A comprehensive comparison of cell seeding methods using highly porous melt electrowriting scaffolds. *Mater. Sci. Eng. C* **2020,** *117*, 111282. DOI: https://doi.org/10.1016/j.msec.2020.111282.

13. Cámara Torres, M.; Sinha, R.; Mota, C.; Moroni, L., Improving cell distribution on 3D additive manufactured scaffolds through engineered seeding media density and viscosity. *Acta Biomater.* **2020,** *101*, 183-195. DOI: https://doi.org/10.1016/j.actbio.2019.11.020.

14. Choi, S. W.; Zhang, Y.; Xia, Y., Three-Dimensional Scaffolds for Tissue Engineering: The Importance of Uniformity in Pore Size and Structure. *Langmuir* **2010,** *26* (24), 19001-19006. DOI: 10.1021/la104206h.

15. Mygind, T.; Stiehler, M.; Baatrup, A.; Li, H.; Zou, X.; Flyvbjerg, A.; Kassem, M.; Bünger, C., Mesenchymal stem cell ingrowth and differentiation on coralline hydroxyapatite scaffolds. *Biomaterials* **2007,** *28* (6), 1036-1047. DOI: https://doi.org/10.1016/j.biomaterials.2006.10.003.

16. Lee, J. W.; Ahn, G.; Kim, J. Y.; Cho, D.-W., Evaluating cell proliferation based on internal pore size and 3D scaffold architecture fabricated using solid freeform fabrication technology. *J Mater Sci Mater Med* **2010,** *21* (12), 3195-3205. DOI: 10.1007/s10856-010-4173-7.

17. Brennan, C. M.; Eichholz, K. F.; Hoey, D. A., The effect of pore size within fibrous scaffolds fabricated using melt electrowriting on human bone marrow stem cell osteogenesis. . *Biomed Mater* **2019** *14*, 065016.

18. Centola, M.; Rainer, A.; Spadaccio, C.; De Porcellinis, S.; Genovese, J. A.; Trombetta, M., Combining electrospinning and fused deposition modeling for the fabrication of a hybrid vascular graft. *Biofabrication* **2010,** *2* (1), 014102. DOI: 10.1088/1758-5082/2/1/014102.

19. Ginestra, P.; Pandini, S.; Ceretti, E., Hybrid multi-layered scaffolds produced via grain extrusion and electrospinning for 3D cell culture tests. *Rapid Prototyp. J.* **2019,** *26* (3), 593-602. DOI: 10.1108/RPJ-03-2019-0079.

20. Kim, G.; Son, J.; Park, S.; Kim, W., Hybrid Process for Fabricating 3D Hierarchical Scaffolds Combining Rapid Prototyping and Electrospinning. *Macromol. Rapid Commun.* **2008,** *29* (19), 1577-1581. DOI: 10.1002/marc.200800277.

21. Lee, H.; Kim, G., Enhanced cellular activities of polycaprolactone/alginate-based cell-laden hierarchical scaffolds for hard tissue engineering applications. *J Colloid Interface Sci* **2014,** *430*, 315-25. DOI: 10.1016/j.jcis.2014.05.065.

22. Lee, H.; Yeo, M.; Ahn, S.; Kang, D. O.; Jang, C. H.; Lee, H.; Park, G. M.; Kim, G. H., Designed hybrid scaffolds consisting of polycaprolactone microstrands and electrospun collagen-nanofibers for bone tissue regeneration. *Journal of biomedical materials research. Part B, Applied biomaterials* **2011,** *97* (2), 263-70. DOI: 10.1002/jbm.b.31809.

23. Martins, A.; Chung, S.; Pedro, A. J.; Sousa, R. A.; Marques, A. P.; Reis, R. L.; Neves, N. M., Hierarchical starch-based fibrous scaffold for bone tissue engineering applications. *J Tissue Eng Regen Med* **2009,** *3* (1), 37-42. DOI: 10.1002/term.132.

24. Moroni, L.; Schotel, R.; Hamann, D.; de Wijn, J. R.; van Blitterswijk, C. A., 3D Fiber-Deposited Electrospun Integrated Scaffolds Enhance Cartilage Tissue Formation. *Adv. Funct. Mater.* **2008,** *18* (1), 53-60. DOI: 10.1002/adfm.200601158.

25. Naghieh, S.; Foroozmehr, E.; Badrossamay, M.; Kharaziha, M., Combinational processing of 3D printing and electrospinning of hierarchical poly(lactic acid)/gelatin-forsterite scaffolds as a biocomposite: Mechanical and biological assessment. *Mater. Des.* **2017,** *133*, 128-135. DOI: https://doi.org/10.1016/j.matdes.2017.07.051.

26. Nandakumar, A.; Barradas, A.; de Boer, J.; Moroni, L.; van Blitterswijk, C.; Habibovic, P., Combining technologies to create bioactive hybrid scaffolds for bone tissue engineering. *Biomatter* **2013,** *3* (2). DOI: 10.4161/biom.23705.

27. Park, S. A.; Kim, H. J.; Lee, S. H.; Lee, J. H.; Kim, H. K.; Yoon, T. R.; Kim, W., Fabrication of nano/microfiber scaffolds using a combination of rapid prototyping and electrospinning systems. *Polym. Eng. Sci.* **2011,** *51* (9), 1883-1890. DOI: 10.1002/pen.21982.

28. Wei, C.; Dong, J., Hybrid hierarchical fabrication of three-dimensional scaffolds. *J. Manuf. Process.* **2014,** *16* (2), 257-263. DOI: https://doi.org/10.1016/j.jmapro.2013.10.003.

29. Yang, G. H.; Mun, F.; Kim, G. H., Direct electrospinning writing for producing 3D hybrid constructs consisting of microfibers and macro-struts for tissue engineering. *Chem. Eng. J.* **2016,** *288*, 648-658. DOI: https://doi.org/10.1016/j.cej.2015.12.047.

30. Yeo, M.; Kim, G., Cell-printed hierarchical scaffolds consisting of micro-sized polycaprolactone (PCL) and electrospun PCL nanofibers/cell-laden alginate struts for tissue regeneration. *J. Mater. Chem. B* **2014,** *2* (3), 314-324. DOI: 10.1039/c3tb21163k.

31. Vyas, C.; Ates, G.; Aslan, E.; Jack Hart, J.; Huang, B.; Bartolo, P., Three-Dimensional Printing and Electrospinning Dual-Scale Polycaprolactone Scaffolds with Low-Density and Oriented Fibers to Promote Cell Alignment. *3D Print Addit Manuf* **2020,** *7* (3), 105-113. DOI: 10.1089/3dp.2019.0091.

32. Gao, Q.; Xie, C.; Wang, P.; Xie, M.; Li, H.; Sun, A.; Fu, J.; He, Y., 3D printed multi-scale scaffolds with ultrafine fibers for providing excellent biocompatibility. *Mater. Sci. Eng. C* **2020,** *107*, 110269. DOI: https://doi.org/10.1016/j.msec.2019.110269.

33. Park, S. H.; Kim, T. G.; Kim, H. C.; Yang, D.-Y.; Park, T. G., Development of dual scale scaffolds via direct polymer melt deposition and electrospinning for applications in tissue regeneration. *Acta Biomater* **2008,** *4* (5), 1198-1207. DOI: https://doi.org/10.1016/j.actbio.2008.03.019.

34. Moroni, L.; Schotel, R.; Hamann, D.; de Wijn, J. R.; van Blitterswijk, C. A., 3D Fiber-Deposited Electrospun Integrated Scaffolds Enhance Cartilage Tissue Formation. *Advanced Functional Materials* **2008,** *18* (1), 53-60. DOI: 10.1002/adfm.200601158.

35. Costa, P. F.; Vaquette, C.; Zhang, Q.; Reis, R. L.; Ivanovski, S.; Hutmacher, D. W., Advanced tissue engineering scaffold design for regeneration of the complex hierarchical periodontal structure. *Journal of Clinical Periodontology* **2014,** *41* (3), 283-294. DOI: 10.1111/jcpe.12214.

36. Vaquette, C.; Ivanovski, S.; Hamlet, S. M.; Hutmacher, D. W., Effect of culture conditions and calcium phosphate coating on ectopic bone formation. *Biomaterials* **2013,** *34* (22), 5538-5551. DOI: 10.1016/j.biomaterials.2013.03.088.

37. Crica, L. E.; Wengenroth, J.; Tiainen, H.; Ionita, M.; Haugen, H. J., Enhanced X-ray absorption for micro-CT analysis of low density polymers. *J. Biomater. Sci. Polym. Ed.* **2016,** *27* (9), 805-823.

38. Olubamiji, A. D.; Izadifar, Z.; Si, J. L.; Cooper, D. M. L.; Eames, B. F.; Chen, D. X. B., Modulating mechanical behaviour of 3D-printed cartilage-mimetic PCL scaffolds: influence of molecular weight and pore geometry. *Biofabrication* **2016** *8*,025020.

39. Zhou, Y.; Hutmacher, D. W.; Varawan, S. L.; Lim, T. M., In vitro bone engineering based on polycaprolactone and polycaprolactone–tricalcium phosphate composites. *Polym. Int.* **2007,** *56* (3), 333-342.

40. Gibson, I. J.; Ashby, M. F., The mechanics of three-dimensional cellular materials. *Proc. R. Soc. Lond. A* **1982,** *382*, 43–59.

41. Karageorgiou, V.; Kaplan, D., Porosity of 3D biomaterial scaffolds and osteogenesis. *Biomaterials* **2005,** *26* (27), 5474-5491. DOI: https://doi.org/10.1016/j.biomaterials.2005.02.002.

42. Yao, Q.; Cosme, J. G. L.; Xu, T.; Miszuk, J. M.; Picciani, P. H. S.; Fong, H.; Sun, H., Three dimensional electrospun PCL/PLA blend nanofibrous scaffolds with significantly improved stem cells osteogenic differentiation and cranial bone formation. *Biomaterials* **2017,** *115*, 115-127. DOI: https://doi.org/10.1016/j.biomaterials.2016.11.018.

43. Kasten, P.; Beyen, I.; Niemeyer, P.; Luginbühl, R.; Bohner, M.; Richter, W., Porosity and pore size of β-tricalcium phosphate scaffold can influence protein production and osteogenic differentiation of human mesenchymal stem cells: An in vitro and in vivo study. *Acta Biomater.* **2008,** *4* (6), 1904-1915. DOI: https://doi.org/10.1016/j.actbio.2008.05.017.

44. Fuchs, A.; Youssef, A.; Seher, A.; Hochleitner, G.; Dalton, P. D.; Hartmann, S.; Brands, R. C.; Muller-Richter, U. D. A.; Linz, C., Medical-grade polycaprolactone scaffolds made by melt electrospinning writing for oral bone regeneration - a pilot study in vitro. *BMC Oral Health* **2019,** *19* (1), 28. DOI: 10.1186/s12903-019-0717-5.

45. Vaquette, C.; Saifzadeh, S.; Farag, A.; Hutmacher, D. W.; Ivanovski, S., Periodontal Tissue Engineering with a Multiphasic Construct and Cell Sheets. *J. Dent. Res.* **2019,** *98* (6), 673-681. DOI: 10.1177/0022034519837967.

46. Huang, B.; Aslan, E.; Jiang, Z.; Daskalakis, E.; Jiao, M.; Aldalbahi, A.; Vyas, C.; Bártolo, P., Engineered dual-scale poly (ε-caprolactone) scaffolds using 3D printing and rotational electrospinning for bone tissue regeneration. *Addit. Manuf.* **2020,** *36*, 101452. DOI: https://doi.org/10.1016/j.addma.2020.101452.

47. Marie, P. J., Role of N-cadherin in bone formation. *J. Cell. Physiol.* **2002,** *190* (3), 297-305. DOI: 10.1002/jcp.10073.

48. Jabalee, J.; Franz-Odendaal, T., Mesenchymal condensation sets the stage for intramembranous bone development. *FASEB J.* **2012,** *26* (S1), 907.7-907.7. DOI: 10.1096/fasebj.26.1_supplement.907.7.

49. Giffin, J. L.; Gaitor, D.; Franz-Odendaal, T. A., The Forgotten Skeletogenic Condensations: A Comparison of Early Skeletal Development Amongst Vertebrates. *J Dev Biol* **2019,** *7* (1), 4. DOI: 10.3390/jdb7010004.

50. Arnsdorf, E. J.; Tummala, P.; Kwon, R. Y.; Jacobs, C. R., Mechanically induced osteogenic differentiation--the role of RhoA, ROCKII and cytoskeletal dynamics. *Journal of cell science* **2009,** *122* (Pt 4), 546-53. DOI: 10.1242/jcs.036293.

51. McBeath, R.; Pirone, D. M.; Nelson, C. M.; Bhadriraju, K.; Chen, C. S., Cell Shape, Cytoskeletal Tension, and RhoA Regulate Stem Cell Lineage Commitment. *Dev. Cell* **2004,** *6* (4), 483-495. DOI: https://doi.org/10.1016/S1534-5807(04)00075-9.

52. Strzelecka-Kiliszek, A.; Mebarek, S.; Roszkowska, M.; Buchet, R.; Magne, D.; Pikula, S., Functions of Rho family of small GTPases and Rho-associated coiled-coil kinases in bone cells during differentiation and mineralization. *BBA-Gen Subjects* **2017,** *1861* (5, Part A), 1009-1023. DOI: https://doi.org/10.1016/j.bbagen.2017.02.005.

53. Huck, K.; Sens, C.; Wuerfel, C.; Zoeller, C.; Nakchbandi, I. A., The Rho GTPase RAC1 in Osteoblasts Controls Their Function. *International journal of molecular sciences* **2020,** *21* (2). DOI: 10.3390/ijms21020385.

54. Ichida, M.; Yui, Y.; Yoshioka, K.; Tanaka, T.; Wakamatsu, T.; Yoshikawa, H.; Itoh, K., Changes in cell migration of mesenchymal cells during osteogenic differentiation. *FEBS letters* **2011,** *585* (24), 4018-24. DOI: 10.1016/j.febslet.2011.11.014.

55. Lane, S. W.; De Vita, S.; Alexander, K. A.; Karaman, R.; Milsom, M. D.; Dorrance, A. M.; Purdon, A.; Louis, L.; Bouxsein, M. L.; Williams, D. A., Rac signaling in osteoblastic cells

is required for normal bone development but is dispensable for hematopoietic development. *Blood* **2012,** *119* (3), 736-744. DOI: 10.1182/blood-2011-07-368753.

56. Shin, H., Fabrication methods of an engineered microenvironment for analysis of cell-biomaterial interactions. *Biomaterials* **2007,** *28* (2), 126-33. DOI: 10.1016/j.biomaterials.2006.08.007.

57. Webster, T. J.; Ergun, C.; Doremus, R. H.; Siegel, R. W.; Bizios, R., Specific proteins mediate enhanced osteoblast adhesion on nanophase ceramics. *Journal of biomedical materials research* **2000,** *51* (3), 475-83.

58. Chen, M.; Patra, P. K.; Lovett, M. L.; Kaplan, D. L.; Bhowmick, S., Role of electrospun fibre diameter and corresponding specific surface area (SSA) on cell attachment. *J Tissue Eng Regen Med* **2009,** *3* (4), 269-79. DOI: 10.1002/term.163.

59. Vaquette, C.; Mitchell, J.; Fernandez-Medina, T.; Kumar, S.; Ivanovski, S., Resorbable additively manufactured scaffold imparts dimensional stability to extraskeletally regenerated bone. *Biomaterials* **2021,** *269*, 120671. DOI: https://doi.org/10.1016/j.biomaterials.2021.120671.

60. Guo, Z.; Ma, M.; Huang, X.; Li, H.; Zhou, C., Effect of fiber diameter on proliferation and differentiation of MC3T3-E1 pre-osteoblasts. *Journal of Biomaterials and Tissue Engineering* **2017,** *7* (2), 162-169. DOI: 10.1166/jbt.2017.1548.

61. Vaquette, C.; Cooper White, J. J., Increasing electrospun scaffold pore size with tailored collectors for improved cell penetration. *Acta Biomater* **2011,** *7* (6), 2544-57. DOI: 10.1016/j.actbio.2011.02.036.

62. Dalton, P. D.; Vaquette, C.; Farrugia, B. L.; Dargaville, T. R.; Brown, T. D.; Hutmacher, D. W., Electrospinning and additive manufacturing: converging technologies. *Biomater. Sci.* **2013,** *1* (2), 171-185. DOI: 10.1039/c2bm00039c.

63. Vaquette, C.; Cooper White, J., A simple method for fabricating 3-D multilayered composite scaffolds. *Acta Biomater* **2013,** *9* (1), 4599-4608. DOI: 10.1016/j.actbio.2012.08.015.

64. Vaquette, C.; Pilipchuk, S. P.; Bartold, P. M.; Hutmacher, D. W.; Giannobile, W. V.; Ivanovski, S., Tissue Engineered Constructs for Periodontal Regeneration: Current Status and Future Perspectives. *Advanced Healthcare Materials* **2018**. DOI: 10.1002/adhm.201800457.

For Table of Content Use Only

The Effect of Dual Pore Size Architecture on *In Vitro* Osteogenic Differentiation in Additively Manufactured Hierarchical Scaffolds

Greeshma Ratheesh, Mengchao Shi, Patrick Lau, Yin Xiao, Cedryck Vaquette

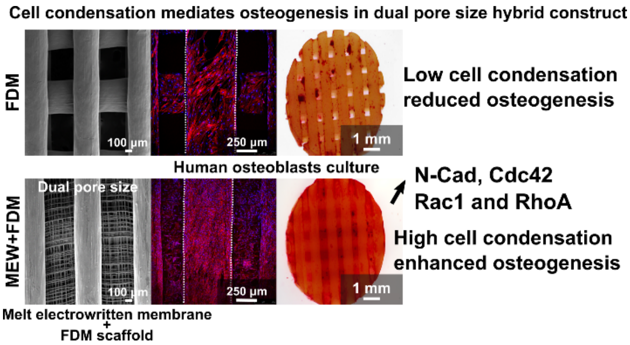

Supplementary information

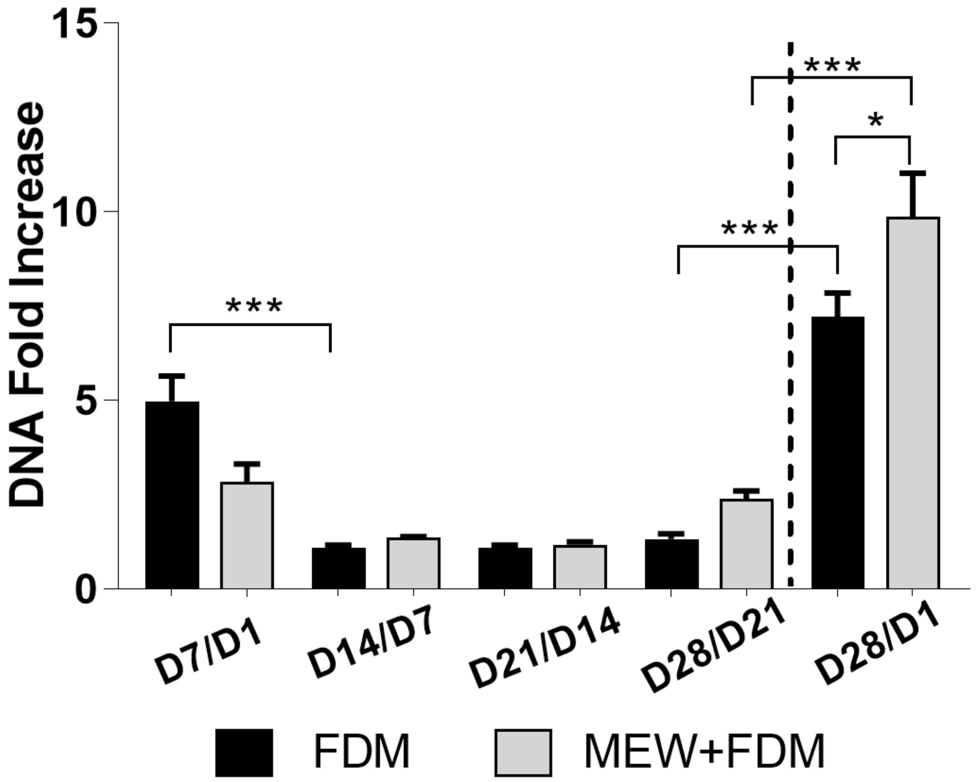

Supplementary Figure 1: Fold change in DNA from the consecutive time points and between the first and last time point.